THE UNIVERSITY of EDINBURGH

Edinburgh Research Explorer

Solubility trapping in formation water as dominant CO2 sink in natural gas fields

Link:
Link to publication record in Edinburgh Research Explorer

Document Version:
Peer reviewed version

Published In:
Nature

OPEN ACCESS

Solubility trapping in formation water as dominant CO2 sink in natural gas fields

Stuart M. V. Gilfillan*, Barbara Sherwood Lollar, Greg Holland, Dave Blagburn, Scott Stevens, Martin Schoell, Martin Cassidy, Zhenju Ding, Zheng Zhou, Georges Lacrampe-Couloume and Chris J. Ballentine

*Author to whom correspondence should be addressed:

Scottish Carbon Capture and Storage, School of GeoSciences, The University of Edinburgh, Grant Institute, The King's Buildings, West Mains Road, Edinburgh, EH9 3JW, UK.

Email: stuart.gilfillan@ed.ac.uk

Injecting CO_2 into deep geological strata is proposed as a safe and economically favourable means to store CO_2 captured from industrial point sources[1-3]. However, it is difficult to assess the long term consequence of CO_2 flooding in the subsurface from decadal observations of existing disposal sites[1,2]. Both the site design and long term safety modelling critically depend on how and where CO_2 will be stored in the site over its lifetime[2-4]. Natural gas fields dominated by a CO_2 phase provide an essential natural analogue for assessing the safety and viability of the geological storage of anthropogenic CO_2 over millennia timescales[1,2,5,6]. Here, we show that the dominant subsurface sink of CO_2 in nine natural gas fields from North America, China and Europe is through dissolution (solubility trapping) in the formation water. All fields, whether siliciclastic or carbonate dominated reservoir lithologies, exhibit a reduction in CO_2 relative to ^3He, an inert and highly insoluble tracer that correlates with an increase in formation water-derived noble gases. Reservoir CO_2 phase loss, sometimes > 90% of that emplaced, is therefore quantitatively related to formation water involvement in the system. $CO_2/^3He$ and $\delta^{13}C(CO_2)$ data for seven gas fields indicate that dissolution in formation water at pH=5-5.8 alone is the major sink for the CO_2 loss. Within two siliciclastic dominated reservoirs some CO_2 loss through precipitation as carbonate minerals cannot be ruled out, but may account for a maximum of 18% loss of the emplaced CO_2. Long term anthropogenic CO_2 storage models in similar geological systems must consider the potential mobility of CO_2 dissolved in water and not geological mineral fixation, which is an insignificant CO_2 trapping mechanism.

Noble gas and CO_2 carbon isotopes are powerful tracers of crustal fluid processes that act on subsurface CO_2[5,7-10]. Within a geological storage site, CO_2 injected as a free CO_2 phase (gas or supercritical) may over time be dissolved in solution (solubility trapping), or locked within carbonate minerals by precipitation (mineral trapping)[4,11]. By using noble gas and carbon

isotope tracers together to study naturally occurring CO_2 systems, we can uniquely identify and quantify the principal mechanism of the CO_2 phase removal, mineral or solubility trapping, over a time scale not accessible through extant injection studies.

We combine noble gas data from five natural CO_2 reservoirs located within the Colorado Plateau and Rocky Mountain provinces, (McCallum Dome, Sheep Mountain, McElmo Dome, CO., Bravo Dome, NM, and St Johns Dome, AZ.)[7] with new $\delta^{13}C(CO_2)$ isotope data (Table 1). Previous work has shown that noble gas patterns in these gas fields are explained by CO_2 gas stripping of the formation water during reservoir filling, followed by partial dissolution of noble gases back into the formation water[7]. We also consider published noble gas and stable isotope information in a further four CO_2-rich natural gas fields (JM-Brown Bassett field (JMBB), Permian Basin, Texas[5]; Kismarja field, Pannonian Basin, Hungary[8]; Jilin field, Jilin Province, Songliao Basin; and Subei Basin field, Jiangsu Province in China[12,13]).

$CO_2/^3He$ ratios within the magmatic range of $1-10x10^9$ have been used to identify a primary magmatic origin of the CO_2 contained within five natural CO_2 reservoirs of the Colorado Plateau and Rocky Mountain Provinces[7]. $CO_2/^3He$ within the Subei Basin and JM-Brown Bassett field also indicate a magmatic origin, whilst the $CO_2/^3He$ values within the Jilin and Kismarja fields are far higher, suggesting a predominantly crustal origin[5,8]. All of the reservoirs exhibit local variation in the CO_2 content relative to the inert tracer ^3He. As there is not a significant source of ^3He within the crust[14], and as ^3He is inert and highly insoluble[9], this variation must be due to changes in the CO_2 component within the reservoirs. While many sources and sinks of CO_2 exist in the subsurface[4,8,9] we argue later that the $CO_2/^3He$ variation is caused by CO_2 loss from the reservoir. The difference between the highest $CO_2/^3He$ and lower values can provide a minimum estimate of this CO_2 loss. In the case of Bravo Dome, a reduction of $CO_2/^3He$ values from $4.82x10^9$ (BD11) to $2.25x10^9$ (BD02)

indicates a >50% loss of the original CO_2 charge in the portion of the reservoir represented by BD02 (Table 1). McElmo Dome samples exhibit a decrease from 8.5×10^9 (YD-1) to 0.68×10^9 (He-2) suggesting >90% emplaced CO_2 loss in portions of this field.

^{4}He is continually produced in the subsurface by the radiogenic decay of U, Th and K[14]. ^{20}Ne is introduced into the subsurface as a component of air dissolved in water and, as such, can only enter the reservoir system via interaction with formation water[9]. While there is no *a-priori* reason to expect a correlation between ^{4}He and ^{20}Ne, this has been observed in natural gases on a regional scale[15]. This correlation is the result of ^{4}He accumulating in the formation water[16] which also contains atmosphere derived ^{20}Ne, and subsequent quantitative partitioning of both ^{4}He and ^{20}Ne into the reservoir phase[7,15]. Almost all CO_2 reservoirs for which we have ^{20}Ne and ^{4}He concentration data show a local ^{20}Ne correlation with ^{4}He (Table 1 and supplementary information). A decrease in $CO_2/^3$He is also correlated with ^{20}Ne in most CO_2 reservoirs (Fig. 1) and with ^{4}He in all CO_2 reservoirs (Fig. 2).

While there are various mechanisms to add crustal CO_2 ($CO_2/^3$He$>>10^{10}$) to these systems[4,10] there is no plausible mechanism that enables crustal CO_2 to be variably added to these systems while preserving a correlation of $CO_2/^3$He with the formation water-derived noble gases. Neglecting small amounts of ^{3}He dissolution back into the formation water[7], changes in $CO_2/^3$He must therefore be due to CO_2 loss in the subsurface via a mechanism directly proportional to the amount of formation water that has been degassed. CO_2 is soluble and reactive. The most likely subsurface CO_2 phase removal mechanisms are solubility and mineral trapping[4,11].

Reservoir lithology may exert a significant influence on how changes in $CO_2/^3$He relate to $\delta^{13}C(CO_2)$. The carbonate reservoirs (McElmo, JMBB, and St. Johns Domes) show little variance in $\delta^{13}C(CO_2)$ whilst the silicilastic fields (Jilin field, Subei Basin, Kismarja, Sheep

Mountain, McCallum and Bravo Domes) exhibit a greater range in $\delta^{13}C(CO_2)$ (Table 1, Supplementary Fig. S1). We consider Bravo and McElmo Domes as case types for each reservoir lithology.

Emplacement of CO_2 at Bravo Dome is believed to have occurred relatively recently (local volcanic activity dates from 8,000-10,000 years)[7,17] and the field may still be undergoing active CO_2 recharge[11]. Decreasing $CO_2/^3He$ within Bravo Dome correlates with more negative $\delta^{13}C(CO_2)$ (Fig. 3a). Taking the highest $CO_2/^3He$ of 4.82 x 10^9 (BD11) to be the sample that experienced the least CO_2 loss, we calculate the coherent change in $CO_2/^3He$ and $\delta^{13}C(CO_2)$ predicted for CO_2 dissolution into the formation water at various pH and for CO_2 precipitation as a carbonate (see Methods Summary). The data are not consistent with precipitation as carbonate being a major sink for CO_2 at Bravo Dome (Figure 3a). However, while a significant number of the data points are consistent with CO_2 dissolution into formation water at a pH between 6-7, it is not possible to rule out a degree of CO_2 loss due to precipitation together with CO_2 dissolution at a lower pH (e.g. pH=5). In such a two process model an upper limit to the proportion of CO_2 lost to precipitation of approximately 18%, can be attributed (Fig. 3a). Hence, in all cases the major CO_2 sink is dissolution. In situ precipitation of 18% reservoir CO_2 would generate between 3.2-6.1% by mass of the whole rock, dependent on whether dolomite, calcite or dawsonite precipitation was favoured by the reservoir conditions. Whilst evidence for CO_2 rich formation water interaction within the reservoir has been documented, to date no secondary carbonate has been identified[18]. Nevertheless, the volume control of the water suggests that the location of the precipitate, if any, is likely to be within the water leg which was not sampled. Lack of reservoir secondary mineralization cannot at this stage rule out any carbonate precipitation as a minor CO_2 sink.

Similar to Bravo Dome, while many of the Sheep Mountain data can be accounted for by dissolution of CO_2 (at pH=5 in this case), a small component of precipitation cannot be ruled out. Adopting the same approach as Bravo Dome, the remaining Sheep Mountain data require a maximum of 10% precipitation and 20% dissolution of the original CO_2 charge (Table 1; Supplementary Fig. S2). In contrast, while minor data scatter may also be due to some small amount of CO_2 precipitation or dissolution at pH=7-8, almost all the data from the other siliciclastic fields of McCallum Dome, Subei basin, Kismarja and the Jilin field can be described by dissolution in the formation water only, within a narrow pH range of between 5-5.3 (Supplementary Figs S3-6).

McElmo Dome carbonate reservoir data show over an order of magnitude change in $CO_2/^3He$ with invariant $\delta^{13}C(CO_2)$ (Figure 3b). This pattern is repeated in the two other carbonate-dominated fields (Supplementary Figures S7, S8). Invariant $\delta^{13}C(CO_2)$ in these fields allows us to discount a two process model of precipitation and dissolution such as at Bravo Dome (Fig. 3a). All data are consistent with CO_2 dissolution into formation water in the pH range of 5.4-5.8 (Figure 3b, Supplementary Figures 7,8), a value similar to the pH obtained for the siliciclastic reservoirs and to values observed (pH=5.7) in carbonate mineral buffered formation water observed in the recent Frio CO_2 injection studies on CO_2 breakthrough[19].

On a reservoir engineering timescale, the early stages of CO_2 injection can result in a drop in pH and dissolution of carbonate minerals into the formation water[18,20-22]. Any significant CO_2 contribution to the reservoir CO_2 phase from re-dissolution of carbonates would be ^3He-free and therefore perturb the $CO_2/^3He$ correlation with ^4He and ^{20}Ne. As there is a clear correlation between $CO_2/^3He$ and ^4He in all fields and ^{20}Ne within the majority, we conclude that dissolution of carbonate minerals into the formation water cannot have had a major influence on $\delta^{13}C(CO_2)$ values. There is no evidence for any precipitation of CO_2 within the

carbonate dominated reservoirs, requiring that the dominant mechanism of reservoir CO_2

loss, up to 90%, is through dissolution into the formation water.

Even the most conservative model we have presented places an upper limit on the CO_2

removed by precipitation at approximately18%, and then only in some samples, from all

natural gas fields investigated in a variety of lithological settings. Precipitation of CO_2 over

millenial timescales represents at most only a small subsurface trapping mechanism for CO_2,

and then only within siliciclastic lithologies. The dominant mechanism of CO_2 loss from

most CO_2 natural gas fields can be accounted for through simple dissolution into the

formation groundwater within a narrow pH window (pH=5-5.8). This study underscores that

geological carbon storage requires careful investigation of existing geologic and

hydrogeologic analogues that have naturally accumulated and stored CO_2 over timescales

relevant to anthropogenic CO_2 storage facilities. We further demonstrate a means of testing

trapping and storage mechanisms via coupled noble gas and carbon isotope measurements in

the context of formation/reservoir water pH evolution.

Methods Summary

Detailed descriptions of the sample collection and analysis procedures can be found in the

original references[5,7,8,21,23]. In our calculations (Figure 3 and Supplemental Figures) we use

the highest $CO_2/^3He$ ratio measured in each field as a reference point to calculate the

correlated reservoir $CO_2/^3He$ and $\delta^{13}C(CO_2)$ ratios as the CO_2 phase is removed by either

precipitation or dissolution. We assume open system loss. In the case of precipitation there is

zero ^3He loss from the CO_2 phase and $CO_2/^3He$ changes in proportion to the fraction of the

remaining CO_2 phase (f). In the case of dissolution the change in $CO_2/^3He$ is calculated

following the Rayleigh equation.

Changes in $\delta^{13}C(CO_2)$ are calculated using the Rayleigh fractionation equation expressed as:

$$\delta^{13}C(CO_2) = \delta^{13}C(CO_2)_o + \varepsilon \ln(f) \text{ [24]}$$

where $\delta^{13}C(CO_2)_o$ is the original system value, f is the fraction of CO_2 remaining in the reservoir, and ε is the carbon isotope fractionation, either for precipitation or for dissolution. Carbon isotope fractionation factors (α) are calculated as a function of temperature for $CO_2(g)$ precipitating to form $CaCO_3(s)$, or dissolving to form either $H_2CO_3(aq)$ or HCO_3^- (aq)[25]. Since all the fractionations are small the simplification can be made that $\varepsilon = 1000\ln(\alpha)$[26]. For typical reservoir waters of pH range 5-8, the contribution of $CO_3^{2-}{}_{(aq)}$ is negligible. Hence for CO_2 dissolution, carbon isotope fractionation between the dissolved inorganic carbon (DIC) pool and CO_2 gas used in the Rayleigh fractionation equation can be expressed as:

$$\varepsilon^{13}C_{DIC-CO2(g)} = x(\varepsilon^{13}C_{H2CO3(aq)-CO2(g)}) + (1-x)(\varepsilon^{13}C_{HCO3^-(aq)-CO2(g)}) \text{ [24]}$$

where x is the proportion of CO_2 gas dissolving to $H_2CO_3(aq)$ at the relevant pH[24].

Solubility as a function of temperature and salinity is given by the IUPAC solubility series for CO_2[27] and by Crovetto et al. and Smith for He[28,29]. The average well depth, reservoir pressure, temperature and salinity are presented in the supplementary information for each reservoir, with the corresponding Henry's Law constants K_{He}, K_{CO2}, and fractionation factor ($1000\ln\alpha$) for $CO_2(g)$ forming $H_2CO_3(aq)$, $HCO_3^-(aq)$ and $CaCO_3(s)$ (Supplemetary Table 1).

References

1   Schrag, D. P. Preparing to Capture Carbon. *Science* **315**, 812-813 (2007).
2   Baines, S. J. & Worden, R. H. in *Geological storage of carbon dioxide* Vol. Special Publication 233 (eds S. J. Baines & R. H. Worden) 1-6 (The Geological Society of London, 2004).
3   Gale, J. in *Geological Storage of Carbon Dioxide* Vol. 233 *Special Publications* (eds S.J. Baines & R.H. Worden) 7-15 (Geological Society, 2004).
4   Bradshaw, J., Boreham, C. & La Pedalina, F. in *Greenhouse Gas Control Technologies, 7th International Conference on Greenhouse Gas Control Technologies* Vol. 1 (eds E. Rubin, D. Keith, & C. Gilboy) 541-550 (Vancouver, 2004).

5   Ballentine, C. J., Schoell, M., Coleman, D. & Cain, B. A. 300-Myr-old magmatic CO_2 in natural gas reservoirs of the west Texas Permian basin. *Nature* **409**, 327-331 (2001).

6   Kintisch, E. The Greening of Synfuels. *Science* **320**, 306-308 (2008).

7   Gilfillan, S. M. V. *et al.* The noble gas geochemistry of natural CO_2 gas reservoirs from the Colorado Plateau and Rocky Mountain provinces, USA. *Geochimica et Cosmochimica Acta* **72**, 1174-1198 (2008).

8   Sherwood Lollar, B., Ballentine, C. J. & O'Nions, R. K. The fate of mantle-derived carbon in a continental sedimentary basin: Integration of C/He relationships and stable isotope signatures. *Geochimica et Cosmochimica Acta* **61**, 2295-2308 (1997).

9   Ballentine, C. J., Burgess, R. & Marty, B. in *Noble Gases in Geochemistry and Cosmochemistry* Vol. 47 *Reviews in Mineralogy & Geochemistry* (eds D. R. Porcelli, C. J. Ballentine, & R. Weiler) 539-614 (2002).

10 Cathles, L. M. & Schoell, M. Modeling CO_2 generation, migration and titration in sedimentary basins. *Geofluids* **7**, 441-450 (2007).

11 Baines, S. J. & Worden, R. H. in *Geological Storage of Carbon Dioxide* Vol. 233 *Special Publications* (eds S.J. Bains & R.H. Worden) 59-85 (Geological Society, 2004).

12 Xu, S., Nakai, S., Wakita, H., Xu, Y. & Wang, X. Carbon isotopes of hydrocarbons and carbon dioxide in natural gases in China. *Journal of Asian Earth Sciences* **15**, 89-101 (1997).

13 Xu, S., Nakai, S., Wakita, H. & Wang, X. Mantle-derived noble gases in natural gases from Songliao Basin, China. *Geochimica et Cosmochimica Acta* **59**, 4675-4683 (1995).

14 Ballentine, C. J. & Burnard, P. G. in *Noble Gases in Geochemistry and Cosmochemistry* Vol. 47 *Reviews in Mineralogy & Geochemistry* (eds D. R. Porcelli, C. J. Ballentine, & R. Weiler) 481-538 (2002).

15 Ballentine, C. J. & Sherwood Lollar, B. Regional groundwater focusing of nitrogen and noble gases into the Hugoton-Panhandle giant gas field, USA. *Geochimica et Cosmochimica Acta* **66**, 2483-2497 (2002).

16 Torgersen, T. & Clarke, W. B. Helium accumulation in groundwater, (i): An evaluation of sources and the continental flux of crustal [4]He in the Great Artesian Basin, Australia. *Geochimica et Cosmochimica Acta* **49**, 1211-1218 (1985).

17 Broadhead, R. F. Natural accumulations of carbon dioxide in the New Mexico region - Where are they, how do they occur and what are the uses for CO_2? *Lite Geology* **20**, 2-6 (1998).

18 Pearce, J. *et al.* Natural occurrences as analogues for the geochemical disposal of carbon dioxide. *Energy Conversion and Management* **37**, 1123-1128 (1996).

19 Kharaka, Y. K. *et al.* Gas-water-rock interactions in Frio Formation following CO_2 injection: Implications for the storage of greenhouse gases in sedimentary basins. *Geology* **34**, 577-580, doi:10.1130/g22357.1 (2006).

20 Knauss, K. G., Johnson, J. W. & Steefel, C. I. Evaluation of the impact of CO_2, co-contaminant gas, aqueous fluid and reservoir rock interactions on the geologic sequestration of CO_2. *Chemical Geology* **217**, 339-350 (2005).

21 Xu, S., Shun'ichi, N., Wakita, H., Xu, Y. & Wang, X. Helium isotope compositions in sedimentary basins in China. *Applied Geochemistry* **10**, 643-656 (1995).

22 Worden, R. H. & Smith, L. K. in *Geological Storage of Carbon Dioxide* Vol. 233 *Special Publications* (eds R. H. Worden & S. J. Baines) 211-224 (Geological Society, London, 2004).

23 Xu, S., Nakai, S., Wakita, H., Yongchang, X. & Xianbin, W. Carbon isotopes of hydrocarbons and carbon dioxide in natural gases in China. *Journal of Asian Earth Sciences* **15**, 89-101 (1997).

24 Clark, I. D. & Fritz, P. *Environmental Isotopes in Hydrology*. (CRC Press, 1997).

25 Deines, P., Langmuir, D. & Harmon, R. S. Stable carbon isotopes and the existence of a gas phase in the evolution of carbonate groundwaters. *Geochimica et Cosmochimica Acta* **38**, 1147 - 1184 (1974).

26 Fritz, P. & Fontes, J. C. *Handbook of Environmental Isotope Geochemistry*. Vol. 1. The Terrestrial Environment (Elsevier Scientific Publishing Company, 1980).

27 Scharlin, P. *IUPAC Solubility Series 62: Carbon Dioxide in Water and Aqueous Electrolyte Solutions*. (1996).

28 Crovetto, R., Fernandez-Prini, R. & Laura Japas, M. Solubilities of inert gases and methane in H_2O and in D_2O in the temperature range of 300 to 600K. *Journal of Chemical Physics* **76**, 1077-1086 (1982).
29 Smith, S. P. Noble gas solubility in water at high temperature. *EOS, Transactions of the American Geophysical Union* **66**, 397 (1985).
30 Sherwood Lollar, B., O'Nions, R. K. & Ballentine, C. J. Helium and neon isotope systematics in carbon dioxide-rich and hydrocarbon-rich gas reservoirs. *Geochimica et Cosmochimica Acta* **58**, 5279 (1994).

Author Contributions S.G., C.B. and B.S.L. designed the study, analysed the samples, interpreted the data and wrote the paper. G.H., D.B., Z.D., Z.Z. and G.L.C. assisted with sample analysis and interpretation of the data. S.S., M.S. and M.C. assisted with sample collection and provided comments on the manuscript.

Author Information Reprints and permissions information is available at www.nature.com/reprints. Correspondence and requests for materials should be addressed to S.G. (stuart.gilfillan@ed.ac.uk).

Table 1: Sample location, Producing formation, major gas species and CO_2 carbon isotopes

Field & Well	Location Twnshp-Rnge/Lat-Long	Producing Formation	$CO_2/^3He$ x 10^9	$^3He/^4He$ (R/R$_a$)	^4He (x 10^{-4}) cm^3(STP)cm^{-3}	^{20}Ne (x 10^{-8}) cm^3(STP)cm^{-3}	$\delta^{13}C(CO_2)$ ‰
Bravo Dome[7]							
BD01	23/19N/34E	Tubb	4.53 (10)	1.670 (8)	0.944 (12)	0.169 (2)	-3.96 (4)
BD02	32/21N/35E	Tubb	2.25 (5)	0.764 (4)	4.15 (5)	0.700 (7)	-4.93 (8)
BD03	36/22N/34E	Tubb	2.41 (5)	0.896 (4)	3.31 (4)	0.521 (5)	-4.89 (19)
BD04	8/20N/34E	Tubb	4.61 (10)	1.611 (8)	0.961 (2)	0.181 (2)	-4.23 (8)
BD05	34/20N/35E	Tubb	2.74 (6)	0.965 (5)	2.70 (4)	0.446 (4)	-4.95 (5)
BD06	26/22N/32E	Tubb	3.94 (8)	1.503 (8)	1.20 (2)	0.202 (2)	-4.55 (11)
BD07	3/19N/33E	Tubb	4.34 (9)	2.104 (11)	0.781 (10)	0.180 (2)	-4.85 (1)
BD08	9/18N/33E	Tubb	3.87 (8)	1.143 (6)	1.61 (2)	0.264 (3)	-3.88 (8)
BD09	17/21N/33E	Tubb	4.22 (9)	1.724 (9)	0.981 (12)	0.180 (2)	-4.44 (11)
BD10	7/22N/34E	Tubb	3.25 (6)	1.104 (6)	1.99 (3)	0.308 (3)	-4.88 (7)
BD11	25/19N/30E	Tubb	4.82 (10)	3.784 (19)	0.391 (5)	0.103 (1)	-3.66 (29)
BD12	27/19N/30E	Tubb	4.74 (10)	3.627 (18)	0.415 (6)		-3.94 (17)
BD13	22/18N/35E	Tubb	3.54 (8)	1.318 (7)	1.53 (2)	0.240 (3)	-4.42 (3)
BD14	16/18N/34E	Tubb	4.39 (9)	1.413 (7)	1.15 (2)	0.179 (4)	-4.04 (2)
BD12b	27/19N/30E	Tubb	4.75 (10)	3.634 (18)	0.413 (6)	0.120 (2)	-3.94 (17)
McCallum Dome[7]							
No. 3 (8-3)	8/9N/78W	Lakota	1.52 (4)	0.354 (7)	12.3 (2)	1.17 (2)	-5.1 (3)
No. 5	3/9N/79W	Lakota	1.04 (3)	0.409 (7)	15.5 (2)	2.71 (3)	-5.2 (1)
No. 36	8/9N/79W	Dakota/Lakota		0.448 (8)	1.32 (12)	8.10 (8)	nm
No. 13	2/9N/79W	Lakota/Morrison	0.89 (2)	0.393 (7)	18.8 (2)	4.36 (5)	-5.3 (2)
No. 79	4/9N/79W	Dakota/Lakota	1.77 (6)	0.406 (6)	9.16 (21)	2.53 (3)	-5.7 (1)
McElmo Dome[7]							
MC-1	37.4155, -108.7713	Leadville	5.04 (11)	0.145 (2)	9.58 (8)	0.376 (4)	-4.26 (10)
HE-2	37.5052, -108.9094	Leadville	0.68 (15)	0.148 (1)	70.5 (7)	0.307 (30)	-4.40 (10)
YC-4	37.4529, -108.8583	Leadville	4.96 (11)	0.137 (3)	10.2 (10)	0.573 (6)	-4.41 (10)
SC-9	37.3934, -108.8733	Leadville	3.17 (7)	0.150 (3)	14.8 (14)	0.497 (5)	-4.29 (10)
YB-2	37.4472, -108.8075	Leadville	8.74 (20)	0.125 (1)	6.42 (61)	0.371 (4)	-4.40 (10)
YC-1	37.4529, -108.8583	Leadville	4.07 (9)	0.142 (2)	12.1 (12)	0.423 (5)	-4.34 (10)
HF-1	37.4871 -108.8807	Leadville	2.16 (6)	0.169 (1)	19.3 (26)	0.564 (12)	-4.37 (10)
HD-2	37.4572, -108.9008	Leadville	4.28 (10)	0.140 (3)	11.7 (12)	0.128 (2)	-4.38 (10)
YA-2	37.4692, -108.7811	Leadville	3.39 (8)	0.138 (3)	15.0 (15)	0.130 (2)	-4.42 (10)
YE-1	37.4818, -108.8123	Leadville	4.16 (9)	0.173 (3)	9.75 (8)	0.143 (3)	-4.45 (10)
HA-1	37.5289, -108.8718	Leadville	4.56 (10)	0.139 (3)	11.0 (11)	0.205 (7)	-4.66 (10)
SC-10	37.3934, -108.8733	Leadville	4.37 (10)	0.139 (2)	11.6 (11)	0.413 (5)	-4.27 (10)
HC-2	37.4734, -108.8860	Leadville	4.68 (11)	0.140 (2)	10.7 (10)	0.409 (6)	-4.38 (10)
HB-1	37.5087, -108.8802	Leadville	4.74 (11)	0.148 (3)	9.94 (10)	0.247 (4)	-4.49 (10)
YD-1	37.4619, -108.8224	Leadville	8.50 (20)	0.145 (3)	5.68 (6)	0.366 (5)	-4.46 (10)
JM Brown Basset[5]							
Turk State No. 1A	30.38758, -101.85642	Ellenberger	5.92 (47)	0.543 (16)	1.25 (9)	nm	-2.88
Bassett Goode No. 3	30.37852, -101.83068	Ellenberger	5.55 (43)	0.527 (16)	1.42 (10)	nm	-2.89
Brown Bassett No. 2*	30.34433, -101.7995	Ellenberger	5.82 (35)	0.502 (15)	1.33 (7)	nm	-2.90
Mayme K. Martin ETAL 1	30.35661, -101.74721	Ellenberger	5.29 (40)	0.372 (11)	1.42 (10)	nm	-2.97
Mitchell 109 No. 2*	30.33329, -101.69826	Ellenberger	4.58 (36)	0.400 (12)	1.53 (11)	nm	-2.92
Mitchell 5 No. 1X	30.32352, -101.68429	Ellenberger	5.61 (43)	0.478 (11)	1.40(10)	nm	-2.84
Mitchell 103 No. 2	30.3568, -101.63642	Ellenberger	4.20 (33)	0.246 (7)	1.39 (10)	nm	-2.70
Mitchell No. 6	30.351, -101.58835	Ellenberger	3.93 (31)	0.264 (8)	1.51 (11)	nm	-2.96
Mitchell No. 3	30.33966, -101.61307	Ellenberger	4.22 (33)	0.240 (7)	1.39 (10)	nm	-3.06
Mitchell A-11 No. 1	30.30286, -101.57677	Ellenberger	4.07 (32)	0.272 (8)	1.66 (12)	nm	-2.93
Mitchell No. 12	30.29118, -101.57295	Ellenberger	4.24 (130)	0.267 (8)	1.46 (10)	nm	-2.96
Sheep Mountain[7]							
8-2-P	2/9-28S/70W	Dakota	2.31 (5)	0.981 (10)	3.13 (3)	1.47 (2)	-5.0 (2)
2-10-O	15/9-27S/70W	Entrada	2.44 (6)	0.984 (12)	2.96 (3)	3.04 (3)	-5.2 (1)
9-26	26/9-27S/70W	Dakota	2.57 (6)	0.934 (14)	2.95 (3)	0.613 (9)	nm
2-9-H	9/9-27S/70W	Dakota	2.44 (6)	0.945 (19)	3.07 (3)	9.77 (10)	nm
3-15-B	15/9-27S/70W	Dakota	2.61 (6)	0.937 (16)	2.90 (3)	1.54 (2)	-5.7 (4)
4-13		Dakota	2.17 (5)	0.942 (18)	3.47 (4)	1.11 (2)	nm
4-26-E	26/9-27S/70W	Entrada	2.20 (5)	1.024 (18)	3.15 (3)	0.442 (4)	-4.8 (1)
3-23-D	22/9-27S/70W	Dakota	2.26 (5)	0.988 (14)	3.17 (3)	0.579 (9)	nm
7-35-L	2/9-28S/70W	Dakota	2.53 (6)	0.916 (14)	3.06 (3)	0.749 (12)	-5.0 (2)
2-35-C	26/9-27S/70W	Dakota	2.57 (6)	0.963 (19)	2.87 (3)	0.573 (8)	nm
1-15-C	15/9-27S/70W	Entrada	2.71 (6)	0.967 (16)	2.71 (3)	6.77 (10)	nm
3-4-O	9/9-27S/70W	Dakota	2.53 (6)	0.937 (14)	2.99 (3)	2.64 (3)	-5.8 (3)
4-14-M	22/9-27S/70W	Dakota	2.65 (6)	0.892 (15)	3.00 (3)	1.11 (1)	nm
5-15-O	22/9-27S/70W	Dakota	2.30 (5)	1.056 (15)	2.92 (3)	4.33 (5)	-5.0 (1)

Field & Well	Location Twnshp-Rnge/Lat-Long	Producing Formation	$CO_2/^3He$ x 10^9	$^3He/^4He$ (R/R$_a$)	^4He (x 10^{-4}) cm^3(STP)cm^{-3}	^{20}Ne (x 10^{-8}) cm^3(STP)cm^{-3}	$\delta^{13}C(CO_2)$ ‰
Sheep Mountain[7]			2.90 (7)				
4-4-P	9/9-27S/70W	Dakota		0.970 (14)	2.52 (2)	1.31 (2)	nm
5-9-A	9/9-27S/70W	Dakota	2.39 (6)	1.006 (18)	2.94 (3)	1.28 (2)	nm
1-1-J	2/9-28S/70W	Dakota	3.61 (8)	0.908 (16)	2.16 (2)	0.878 (12)	-5.2 (1)
1-22-H	22/9-28S/70W	Entrada	2.25 (5)	0.981 (17)	3.22 (3)	0.937 (13)	-4.5 (2)
St. Johns Dome[7]							
22-1X	34.4265, -109.2664	Supai	0.098 (2)	0.455 (8)	134 (13)	34.4 (47)	-3.65 (5)
10-22	34.2437, -109.1645	Supai	1.91 (42)	0.394 (8)	9.42 (9)	2.30 (4)	-3.79 (5)
3-1	34.3771, -109.2563	Supai	0.22 (3)	0.433 (9)	70.6 (7)	15.1 (21)	-3.85 (5)
Jillin Field[12, 13, 23]							
Wan 2		Cretaceous	1.44 (4)	4.91 (6)	1.00 (2)	nm	-3.6
Wan 5		Cretaceous	227 (7)	4.10 (4)	0.0076 (2)	0.0547 (15)	-5.0
Wan 6		Cretaceous	8.32 (3)	4.99 (5)	0.169 (4)	0.230 (6)	-3.8
Wan 8		Cretaceous	nm	4.30 (5)	nm	nm	-3.2
Wan 9		Cretaceous	36.6 (10)	4.08 (4)	0.047 (1)	0.130 (3)	-3.8
Subai Basin[12, 23]							
Huangqyan 1		Permian	2.17 (7)	3.52 (5)	3.13 (3)	1.47 (2)	-3.6
Sutail 74		Devonian	0.493 (14)	3.59 (4)	2.96 (3)	3.04 (3)	-4.1
Su203		Eocene	0.459 (13)	2.61 (3)	2.95 (3)	0.613 (9)	-2.7
Kismarja[8,30]							
Kismarja 8		Up. Pannonian	20.2 (5)	1.33 (3)	0.226 (7)	nm	-5.0
Kismarja 79		Up. Pannonian	15.5 (4)	1.38 (3)	0.310 (10)	nm	-4.9
Kismarja 61		Up. Pannonian	27.3 (6)	1.16 (2)	0.205 (6)	nm	-5.1
Kismarja 55		Up. Pannonian	13.3 (3)	1.38 (3)	0.360 (11)	nm	-5.1
Kismarja 56		Up. Pannonian	1090 (3)	1.16 (2)	0.0052 (2)	nm	-6.8
Kismarja 74		Up. Pannonian	65.2 (2)	1.34 (3)	0.078 (3)	nm	-6.4
Kismarja 22		Up. Pannonian	1.52 (1)	1.02 (2)	1.31 (3)	nm	-6.6

nm = not measured   1σ error shown in brackets

**Figure Captions**

Figure 1. $CO_2/{}^3He$ variation plotted against ${}^{20}Ne$ in samples from the 'global' data set of CO_2-rich natural gas fields (see text). There is a general trend in this data set of decreasing $CO_2/{}^3He$ with increasing ${}^{20}Ne$. This trend is most clearly apparent in the siliciclastic case type Bravo Dome data set (inset) but less clear in the carbonate case type reservoir, McElmo Dome (inset). ${}^3He$ is conservative within the gas phase. Lower $CO_2/{}^3He$ therefore represent subsurface reduction in CO_2 concentration in the emplaced CO_2 phase. Since the only subsurface source of the ${}^{20}Ne$ now in the CO_2 phase is the formation water, the CO_2 sink must be linked to the formation water contacted by the gas phase.

Figure 2. The 'global' data sets of CO_2 gas fields also show a strong correlation between decreasing $CO_2/{}^3He$ and increasing ${}^4He$ concentration. ${}^4He$ accumulates in formation water over time[7,15,16] and underscores the importance of formation water in controlling the mechanism of subsurface CO_2 removal (Fig.1 and text). We speculate that the formation water ${}^4He$ signature with $CO_2/{}^3He$ is more coherent than the ${}^{20}Ne$ (Fig. 1) due to perturbation of ${}^{20}Ne$ in ancient formation water through non-water phase interaction[9] with subsequent ${}^4He$ accumulation providing a homogenous regional scale formation water ${}^4He$ signal[15,16]. Different $CO_2/{}^3He$ vs. ${}^4He$ gradients will be due to different local formation water ${}^4He$ accumulation rates.

Figure 3. $\delta^{13}C(CO_2)$ against $CO_2/{}^3He$ for Bravo Dome (Top) and McElmo Dome (Bottom) Error bars are 1σ. Top Panel: The solid line shows the predicted trend for carbonate mineral precipitation and the dashed lines show $CO_2(g)$ dissolution trends

for varying formation water pH (see methods). Bravo Dome data is not consistent with the major CO_2 sink being precipitation of carbonate (see text). Bottom Panel: Invariant $\delta^{13}C(CO_2)$ with over an order of magnitude change in $CO_2/^3He$ in McElmo Dome gases cannot be accounted for by precipitation (solid line). Dissolution of reservoir CO_2 into formation water at pH=5.6 would produce the observed results (see text).

Bravo Dome

McElmo Dome
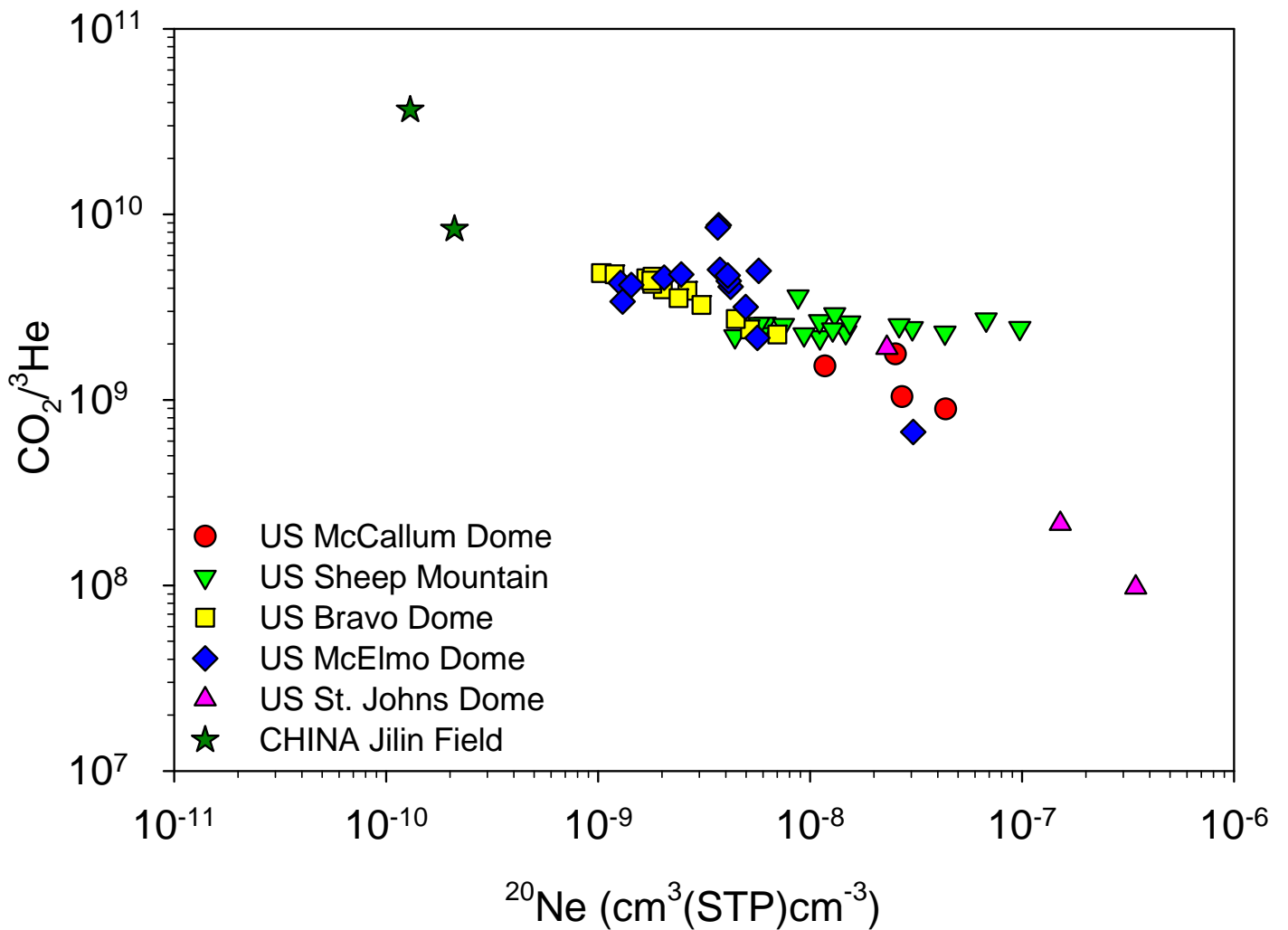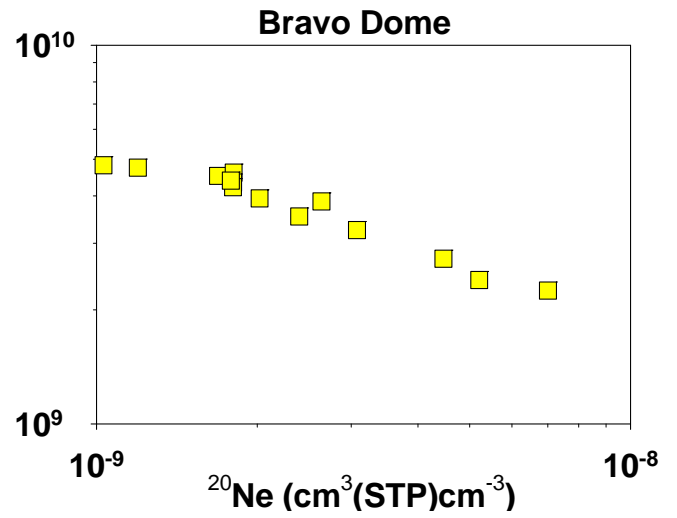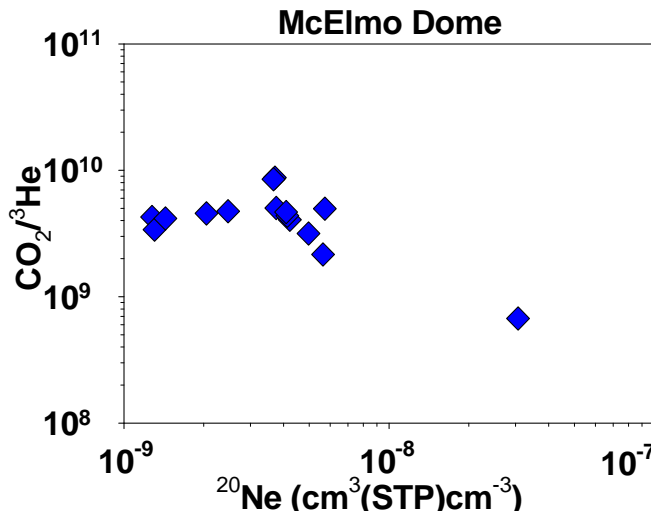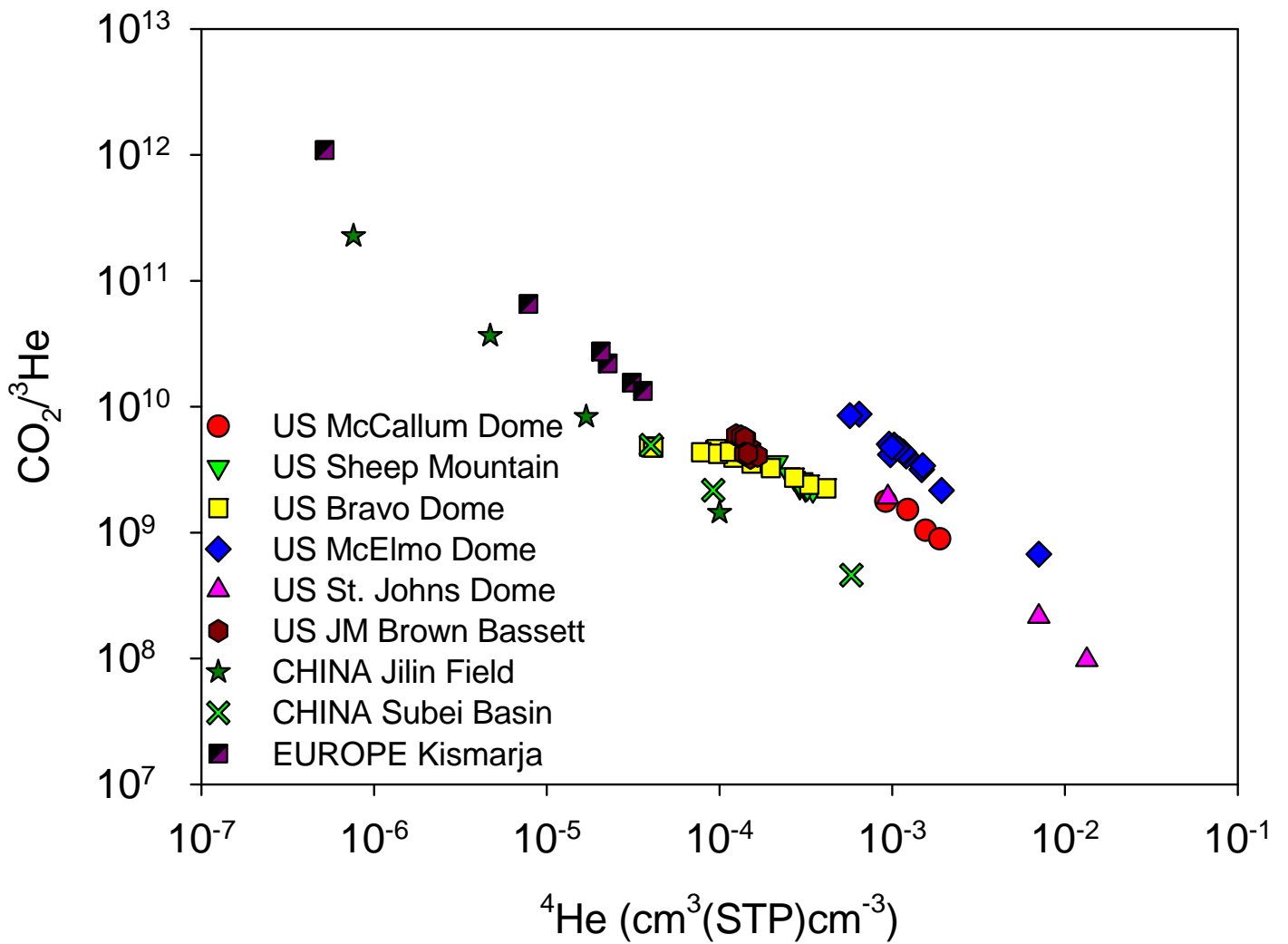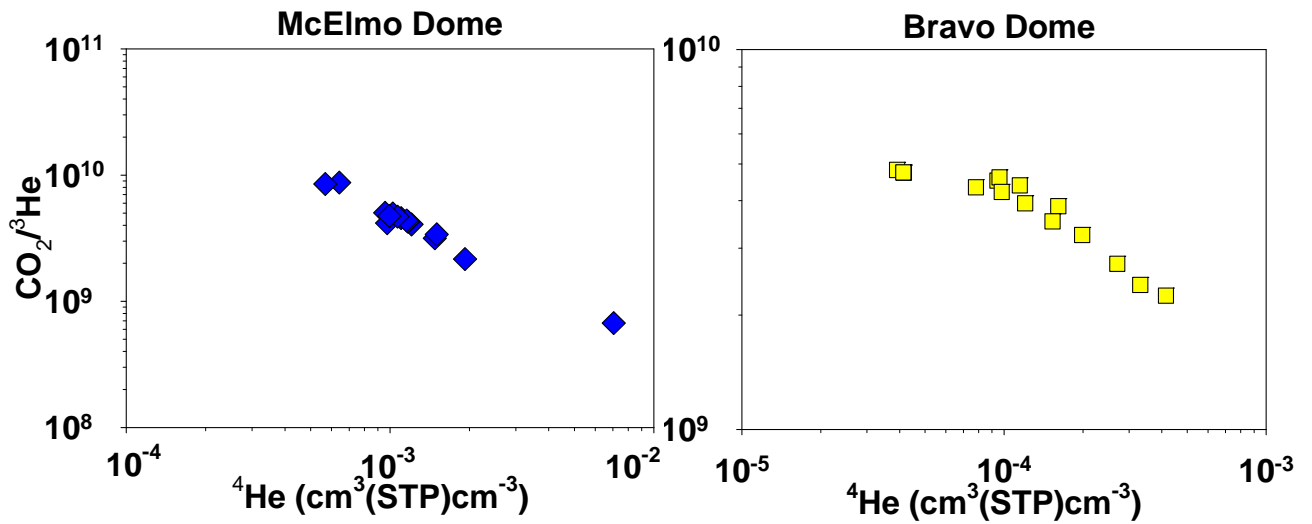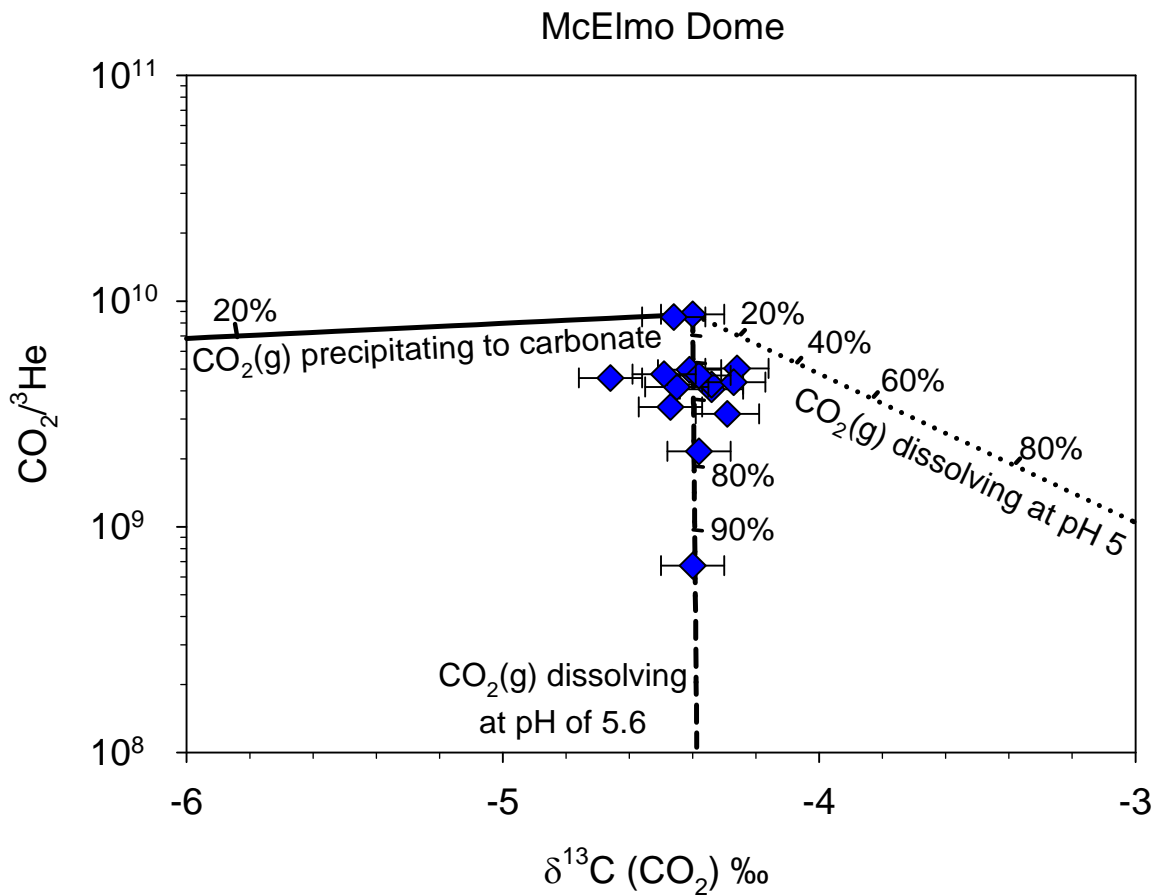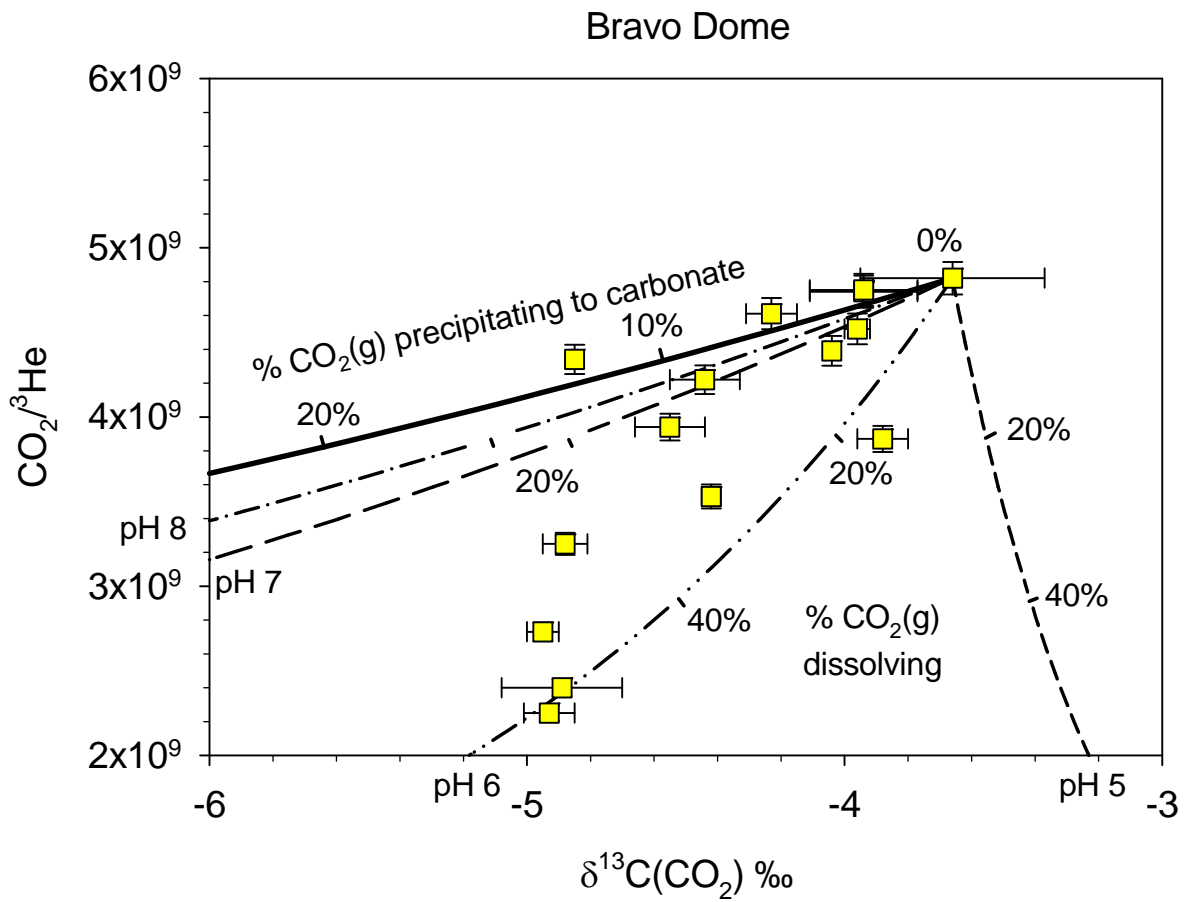
Supplementary Information:

Supplementary Table 1
Reservoir Conditions Used in Models

Reservoir	Average Well Depth (m)	Pressure (MPa)	Borehole Temperature (K)	TDS (molar)	K_{He} (GPa)	K_{CO2} (GPa)	Fractionation (1000lnα) for $CO_{2(g)}$ forming (‰) [24]		
							$H_2CO_{3(aq)}$	HCO_3^-	$CaCO_3$
Bravo Dome[30]	820	8.03	314	1.45	20.1	0.349	-0.846	6.63	8.55
JM Brown Bassett[5]	2800*	27.4*	373	1.00*	14.0	0.774	-0.864	3.36	4.96
McCallum Dome[7]	1630	16.0	338	0.228	14.1	0.460	-0.854	5.10	6.85
McElmo Dome[7]	2450	24.0	344	0.200	11.9	0.487	-0.856	4.76	6.48
Sheep Mountain[7]	1400	13.7	331	0.0137	13.6	0.438	-0.852	5.51	7.29
St. Johns Dome[31]	630	6.17	322	0.0720	14.4	0.281	-0.849	6.08	7.92
Jilin Field[21]	840	8.23	333*	1.00*	17.4	0.491	-0.853	5.39	7.16
Subei Basin[12]	2251	22.1	357*	1.00*	15.4	0.665	-0.860	4.09	5.75
Kismarja[29]	825	8.08	326*	1.00*	17.7	0.438	-0.850	5.82	7.63

*JM Brown Bassett depth estimated from bottom hole temperature and 30°C/km geothermal gradient. Jilin Field, Subei Basin and Kismarja borehole temperatures estimated from depth and geothermal gradient. JM Brown Bassett, Jilin Field, Subei Basin and Kismarja salinity estimated.

Additional References for Supplementary Table

30. Broadhead, R. F. Carbon dioxide in northest New Mexico. *West Texas Geological Society Bulletin* **32**, 5-8 (1993).

31. Stevens, S. H., Fox, C., White, T. & Melzer, S. Natural CO_2 analogs for Carbon Sequestration. *Final Report for USDOE* (2006).